Extreme Poisson's ratios and their electronic origin in B2 CsCl-type AB intermetallic compounds

X. F. Wang,[1,2] Travis E. Jones,[3,*] W. Li,[1,2] and Y. C. Zhou[1,†]

[1]*Key Laboratory of Low Dimensional Materials & Application Technology (Ministry of Education), Xiangtan University, Hunan 411105, China*

[2]*Faculty of Material and Photoelectronic Physics, Xiangtan University, Hunan 411105, China*

[3]*Molecular Theory Group, Colorado School of Mines, Golden, Colorado 80401, USA*

(Received 4 January 2012; revised manuscript received 15 March 2012; published 23 April 2012)

Negative Poisson's ratios have been observed in a variety of metals and alloys. However, the electronic origin of this effect remains unclear, as is evident by our limited knowledge about intermetallics showing this behavior. In an effort to clarify the electronic origin of a negative Poisson's ratio, we have performed a systematic and comprehensive study of extreme (both positive and negative) Poisson's ratios behavior in the B2 CsCl-type AB intermetallic family (including 14 common intermetallics and 128 rare-earth-metal transition or main-group-metal intermetallics) by way of density functional theory calculations. We found a pronounced correlation between the extreme Poisson's ratios and the elastic anisotropy, with approximately 70% of the B2 intermetallics showing intrinsic auxetic behavior. We went on to examine the topology and geometry of the electron charge density and found that the extreme Poisson's ratios are attributable to the directionality of the bonds of the material. Auxetic materials were found to have nondirectional bonds, and nonauxetic compounds had directional bonds. Our findings provide an essential electronic perspective to forecast the auxetic behavior, and suggest a new application for intermetallic compounds.

DOI: 10.1103/PhysRevB.85.134108 PACS number(s): 62.20.dj, 62.20.de, 81.05.Bx

I. INTRODUCTION

While everyday experience suggests that when a material is stretched in one direction it becomes thinner in the perpendicular directions, lateral extension in response to a longitudinal tensile strain is not forbidden by thermodynamics. In fact, such negative Poisson's ratios are observed in many solids.[1,2] Materials that exhibit this novel and counterintuitive behavior, now characterized as auxetic materials, have a wide range of potential technological applications such as electrodes that amplify the response of piezoelectric sensors, aircraft gas turbine engines, improved honeycomb dielectrics, self-adaptive vibration damping materials, improved sound and shock absorption materials, and artery dilators.[1,3,4] Early reported auxetic materials relied heavily on their re-entrant geometries, which should be tailored by deliberate design of material architecture.[5,6] Since then, auxetic behavior has been observed in single-crystal materials including elemental metals, alloys, and metal oxides.[3,4,7,8] For example, Baughman *et al.* showed that 69% of the cubic elemental metals have negative Poisson's ratios, and their auxetic behavior can be correlated with their work functions.[4] These crystals are regarded as intrinsically auxetic materials because the auxetic behavior of the defect-free structure is a result of atomic/electronic structure of the material. Thus, the elastic deformation mechanisms of their internal atomic structure have attracted the interest of many researchers.[1] For the elemental metals, a mechanism based on interactions between hard spheres in specific crystal planes can give rise to auxetic behavior.[4] However, this mechanism only considers the rigid action between hard spheres, disregarding the effect of the electronic structure. Such a mechanism can not suitably describe the auxetic behavior of alloys. Despite the utility of these materials and the lack of a fundamental understanding of the role of electronic structure in auxetic behavior, reports exploring the relationship between electronic structure and the auxetic property of alloys are still scarce. Here, we present one such study using the simplest intermetallic alloys, the B2 CsCl-type AB intermetallic compounds.

The B2 CsCl-type AB intermetallics have generated significant interest for their superior mechanical properties, and are being, or will be, utilized in applications which include aerospace, industrial, and commercial materials. Ample research has focused on the mechanical properties of this intermetallic family, especially the plastic deformation mechanisms, including stain-induced martensitic transformation paths[9] and defect energies calculations.[10–14] For example, B2 TiNi exhibits a reversible martensitic transformation from a B2 to a B19′ structure making it a shape-memory alloy, which is an important alloy for medical devices such as surgical tools, coronary probes, and stints.[9,15,16] The B2 phase of CuZr plays a crucial role in the transformation-mediated ductility of CuZr-based bulk metallic glass (BMG) composites. It greatly improves the ductility BMG composites with working-hardening capability and may turn BMGs into reliable structural materials.[17–19] And while until recently the binary B2 intermetallics were considered to be brittle, a new class of ductile RM (where R = a rare-earth and M = a main-group or transition metal) intermetallics was discovered by Gschneidner *et al.* in 2003.[14] Of the approximately 150 reported RM intermetallic compounds, few are brittle, providing a good opportunity to further our understanding of the nature of the mechanical behavior of intermetallics.[10–13,20] However, the elastic response of these materials has yet to be systematically investigated. Specifically, independent elastic constants for most B2 intermetallics have not been obtained, whether auxetic behavior occurs in these alloys has not been confirmed, and the intrinsic origin of their elastic response is unknown. This paper addresses these questions from the perspective of electronic-structure theory.

While the elastic response of an alloy is determined by its electronic structure, the structure-property relationships that

describe an alloy's elastic properties by way of its chemical bonds are incomplete because traditional pictures of bonding fail to explain the mechanical properties of materials.[21–25] A fundamental understanding of the electronic origins of elastic response is, however, crucial to form a complete picture of mechanical behavior. Such a picture can be found in the electron charge density, which is a quantum mechanical observable.

The Hohenburg-Kohn theorem posits that all ground-state properties are a consequence of the electron charge density,[26] which has led researchers to search for the relationship between a materials charge density and its properties.[27–29] Eberhart and Jones have demonstrated that an extension of Baders topological theory of molecular structure, the quantum theory of atoms in molecules (QTAIM),[28] can be used to calculate the properties of individual bonds, and hence predict mechanical properties of materials.[30–32] While calculating the properties of these topological bonding volumes can be difficult, they can often be approximated by the geometry of the charge density at its topological bond points. By way of example, Eberhart has shown that a strong correlation exists between the geometry of the total electron density $\rho(\vec{r})$ at its topological bond points and elastic constants in fcc metals.[21] Eberhart and Jones have extended this work to alloys and defects and discussed the relationship between the charge density topology and geometry and the mechanical properties for various alloys and defects.[21–25,33–35] For instance, charge density shear moduli relationships for dilute substitutional solution AlLi alloys,[24] and relationships between dislocation glide in bcc metals and the topology of the charge density at the dislocation cores,[22] have been studied. The success of this theory makes it an attractive starting point to probe the electronic origin of auxetic behavior in B2 intermetallic compounds.

The remainder of the paper is organized as follows. The computational methodologies employed in the current study are given in Sec. II. Single-crystal elastic constants of the B2 intermetallics are listed in Sec. III A. Section III B contains a derivation of the method for calculating the extreme (both positive and negative) Poisson's ratios in cubic crystals. The elastic anisotropy and extreme Poisson's ratios, and their relationships for B2 intermetallic compounds, are presented in Sec. III C. Then, in Sec. III D, we report the details of the analysis of the charge density of the B2 intermetallic compounds and the resultant structure-property relationships describing extreme Poisson's ratios of B2 intermetallic compounds. Finally, conclusions and acknowledgments are given in Sec. IV.

II. METHODOLOGY

In order to systematically explore the auxetic behavior of B2 CsCl-type intermetallic compounds, we investigated 142 sets of elastic constants of B2 CsCl-type intermetallics, including 14 common B2 intermetallics and 128 known B2 CsCl-type RM (R = rare-earth elements, M = metallic elements from groups 2, 8–13) intermetallic compounds.[14,20] The details of the B2 CsCl-type RM alloys are summarized as a Periodic Table of the elements in Fig. 1.

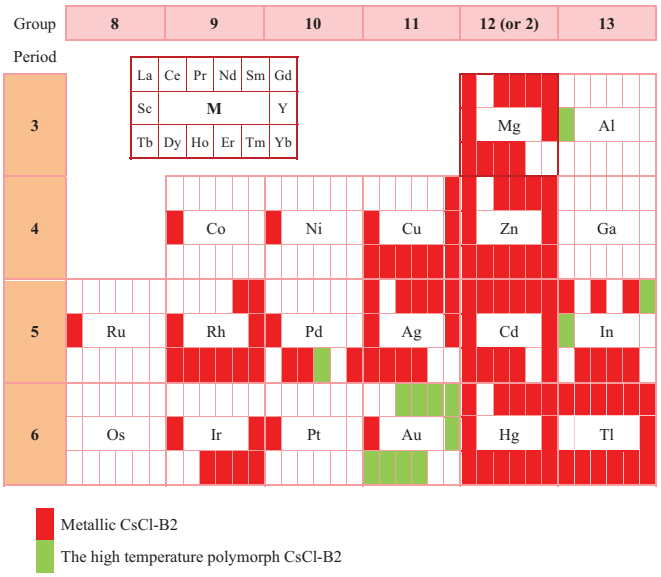

FIG. 1. (Color online) The diagram of present investigated alloys in the B2 RM intermetallics, which are arranged in a partial section of the Periodic Table from groups 2 and 8–13.

A. *Ab initio* calculations of elastic constants of the B2 intermetallics

The *ab initio* calculations were carried out using the Vienna *ab initio* simulation package (VASP),[36] which solves the electronic band structure based on the density functional theory (DFT).[37] Because of the presence of rare-earth elements, the projector augmented plane-wave (PAW) pseudopotential supplied by VASP was used,[38] the validity for RM binary alloys of which has been widely verified.[39,40] Some rare-earth elements, such as Eu and Lu, generated erroneous results and were not included in this work, due to the itinerant nature of the f electrons and the difficulty of calculating their energies accurately in DFT.[39,41] The exchange and correlation energy was treated within the generalized gradient approximation of Perdew-Wang 91 (GGA-PW91).[42] For comparison, another generalized gradient approximation, the Perdew, Burke, and Ernzerhof (GGA-PBE), was also employed.[43] There are three versions of potentials for rare-earth elements in VASP, i.e., the standard version, the divalent version, and the trivalent version. In order to ensure the correctness of the calculations in this study, the choice of these potentials was made following the discussions in Refs. 40 and 44. The wave functions were expanded in a plane-wave basis with a cutoff energy of 500 eV. The k-point sampling in the Brillouin zone (BZ) of the crystalline B2 cubic lattice was treated with the Monkhorst-Pack scheme,[45] using a $15 \times 15 \times 15$ k-point mesh for the geometry optimization and a $21 \times 21 \times 21$ k-point mesh for the static calculation. All calculations were performed using the accurate setting within VASP to avoid wraparound errors.

For a cubic crystal, there are only three independent nonzero elastic constants in the contracted Voigt notation: they are C_{11}, C_{12}, and C_{44}. They can be computed from the curvature of the internal energy versus strain curves when the appropriate strains are chosen. These three modes and their nonzero strain states adopted here are as follows:[46] (1) $\epsilon_{11} = \epsilon_{22} = \gamma$,

$\epsilon_{33} = (1+\gamma)^{-2} - 1$; (2) $\epsilon_{11} = \epsilon_{22} = \epsilon_{33} = \gamma$; and (3) $\epsilon_{12} = \epsilon_{21} = \gamma/2$, $\epsilon_{33} = \gamma^2/(4-\gamma^2)$. Deformation magnitudes γ from -0.012 to 0.012 in steps of 0.003 were applied in the first and second strain modes, γ from -0.04 to 0.04 in steps of 0.01 were adopted in the third strain mode. There is a second common form of the third strain mode, which is related to C_{44}, and can be expressed as $\epsilon_{12} = \epsilon_{23} = \epsilon_{31} = \gamma$.[47] We compared the calculated values of C_{44} for CuY and AgY, as well as 14 common B2 intermetallics, using the two different strains and found no appreciable differences. We chose to use only the second strain mode for the remainder of this work.

B. Analysis of charge density topologies and geometries

In order to analyze the relationship between the electron charge density and the elastic properties of the B2 intermetallic compounds, we used TECPLOT to locate the critical points of the total electron charge density and calculate the Hessian at those points.[48] We employed a fine charge density grid, approximately 25 points per angstrom, to ensure convergence of the derivatives.

III. RESULTS AND DISCUSSION

A. Single-crystal elastic properties of B2 intermetallics

Table I lists the calculated and measured single-crystal elastic constants of the common B2 intermetallics (including CuY and AgY).[14,15,49–57] The calculated elastic constants of the 128 B2 *RM* intermetallics are tabulated in the Supplemental Material available online (Table S).[58] The requirements of mechanical stability in a cubic crystal are $(C_{11} + 2C_{12}) > 0$, $(C_{11} - C_{12}) > 0$, $C_{44} > 0$. All of the C_{ijs} $(i, j = 1, 1; 1, 2; 4, 4)$ values for B2 intermetallics satisfy these criteria.

At this point, it should be noted that at 0 K, the temperature at which the DFT calculations were performed, some of these systems are mechanically unstable due to a soft mode off the Γ point.[59–62] In an effort to obtain elastic moduli comparable with those measured at finite temperature, we suppressed this soft mode by performing our total energy calculations on two-atom unit cells. The calculated, symmetry-suppressed *elastic constants* are generally in good agreement with the observed high-temperature values. Inspection of Table I shows that most of our data are within ±5% of previously reported results. In the worst case, NiTi, our calculated C_{11}, C_{12}, and C_{44} differ from experimental data measured at 298 K (Ref. 53) by 9%, 21%, and 34%, respectively.

The generally good agreement between the measured elastic moduli and the calculated symmetry-suppressed moduli seen here can be justified by considering that the change in elastic moduli with temperature is primarily influenced by changes in volume.[63,64] In most systems, the $T = 0$ K lattice constant found using modern GGAs is in excellent agreement with experimentally measured finite-temperature lattice constants,[36,38–44,65] making the $T = 0$ K total energy calculation of elastic moduli accurate on average, although outliers such as NiTi may be present.

Inspection of Table I reveals that the C_{ijs} we calculated using PAW pseudopotentials with GGA show an improvement over results obtained using ultrasoft pseudopotentials with GGA, and the same precision as results found by way of the full-potential linearized augmented plane-wave (FLAPW) method. Furthermore, one can see from the results in Table I and Table S there is only a small discrepancy between GGA-PW91 and GGA-PBE, suggesting that our calculated elastic moduli are robust and reliable.

B. Extreme Poisson's ratios of B2 intermetallics

For specified directions, the Poisson's ratio (PR) is $\upsilon(\vec{n},\vec{m}) = \epsilon_{\vec{m}}\epsilon_{\vec{n}}$, where $\epsilon_{\vec{m}}$ is a lateral contraction in direction $\vec{m}$ and $\epsilon_{\vec{n}}$ is the longitudinal extension in direction $\vec{n}$ during the stretching of a body, respectively. Once the single-crystal independent elastic constants of the B2 intermetallics are obtained, Poisson's ratio can be expressed in terms of the elastic constants or the elastic compliances. The general formula for the PR of cubic material in a directional $(\vec{n},\vec{m})$, in terms of the elastic constants, has been given by Paszkiewicz *et al.*:[66]

$$\upsilon(\vec{n},\vec{m}) = \frac{(C_{11}+2C_{12})(C_{11}-C_{12}-2C_{44})D(\vec{n},\vec{m}) + 2C_{12}C_{44}}{2(C_{11}+2C_{12})(C_{11}-C_{12})C_{44}}E(\vec{n}), \tag{1}$$

where $E(\vec{n})$ is Youngs modulus,

$$\frac{1}{E(\vec{n})} = \frac{1}{3(C_{11}+2C_{12})} - \frac{1-3P(\vec{n})}{3(C_{11}-C_{12})} + \frac{1-P(\vec{n})}{2C_{44}}. \tag{2}$$

$D(\vec{n},\vec{m}) = n_1^2m_1^2 + n_2^2m_2^2 + n_3^2m_3^2$ and $P(\vec{n}) = n_1^4 + n_2^4 + n_3^4$ are the two functions of the $\vec{n}$ and $\vec{m}$ directions for directional dependence of PR. Considering that the $\vec{n}$ and $\vec{m}$ vectors are mutually orthogonal, we can rewrite them in spherical coordinates to express $D(\vec{n},\vec{m})$ and $P(\vec{n})$ as

$$D(\vec{n},\vec{m}) = \frac{\cos^2(\beta)[\cos^2(\alpha)\cos^2(u) + \sin^2(\alpha)\sin^2(u)]}{1+\tan^2(w)} + \frac{\sin^2(\beta)\tan^2(w)}{1+\tan^2(w)}, \tag{3}$$

$$P(\vec{n}) = \cos^4(\beta)\left[1 - \frac{1}{2}\sin^2(2\alpha)\right] + \sin^4(\beta), \tag{4}$$

$$\tan(w) = -\frac{\cos(\alpha)\cos(u) + \sin(\alpha)\sin(u)}{\tan(\beta)}, \tag{5}$$

where α (or u) is the azimuthal angle and β (or w) is the polar angle in spherical coordinate system, corresponding to the $\vec{n}$ (or $\vec{m}$) direction in the orthogonal coordinate system, respectively. The PRs in arbitrary direction can be obtained via three variables, α, β, u with expressions (1)–(5). We can

TABLE I. A comparison of *ab initio* elastic properties (including bulk modulus K) of selected B2 intermetallics (this study) with the available reported data.

Alloy	C_{11} (GPa)	C_{12} (GPa)	C_{44} (GPa)	K (GPa)	v_{min}	v_{max}	A	Ref.
CuZr	139.2	111.4	44.7	120.7	− 0.2	0.9	3.6	a
	137.3	108.9	44.9	118.4	− 0.1	0.9	3.2	b
	138.0	112.0	45.0	120.6	− 0.1	0.9	3.5	c[49]
TiZn	140.7	107.2	97.0	116.9	− 0.4	1.1	5.8	a
	140.6	106.2	99.2	117.6	− 0.4	1.1	5.8	b
	143.5	99.0	94.0	113.8	− 0.3	0.9	4.2	c[50]
				109.0				d[50]
NiTi	176.5	156.1	46.8	162.9	− 0.2	1.1	4.6	a
	179.5	156.4	49.5	164.1	− 0.2	1.1	4.3	b
	183.0	146.0	46.0	159.0	0.0	0.8	2.5	c[15]
	178.2	147.6	49.0	143.7	− 0.1	0.9	3.2	c[51]
	162.4	129.2	34.8	126.0	0.1	0.7	4.0	d[53]
AlZr	145.4	85.2	27.1	105.3	0.3	0.4	0.9	a
	145.7	86.2	29.8	106.0	0.4	0.4	1.0	b
				103.2				c[52]
CuZn	121.7	110.3	80.7	114.1	− 0.7	1.5	14.2	a
	123.4	110.9	84.3	115.1	− 0.7	1.5	13.5	b
	120	117	80		− 0.9	1.8		d[54]
	140	110	85		− 0.4	1.1		d[55]
AgMg	80.9	56.6	47.4	64.7	− 0.2	0.9	3.9	a
	79.8	55.5	47.8	63.6	− 0.2	0.9	3.9	b
					− 0.2	0.8		d[56]
AgZn	97.1	88.7	51.8	91.5	− 0.6	1.5	12.4	a
	97.3	88.0	54.0	91.1	− 0.6	1.5	11.5	b
AgCd	78.3	74.9	44.5	76.0	− 0.8	1.7	25.8	a
	76.8	72.7	45.1	74.1	− 0.8	1.7	22.3	b
AuZn	123.7	113.9	44.0	117.2	− 0.5	1.4	9.0	a
	124.1	113.5	46.8	117.0	− 0.5	1.4	8.8	b
					− 0.43	1.28		d[56]
					− 0.52	1.38		d[56]
	147.4	133.9	62.2		− 0.5	1.4	9.2	d[57]
AuCd	93.2	91.6	38.4	92.4	− 0.9	1.9	45.2	a
	91.8	89.9	39.6	90.6	− 0.9	1.8	42.8	b
					− 0.7	1.57		d[3]
AlTi	150.3	96.2	68.4	114.2	− 0.1	0.7	2.5	a
	150.9	97.6	70.1	115.4	− 0.1	0.7	2.6	b
				109.7				c[52]
NiAl	210.1	135.8	115.9	158.6	− 0.2	0.7	3.1	a
	207.0	116.4	106.8	157.9	− 0.2	0.7	3.2	b
PtTi	203.8	181.2	46.9	188.7	− 0.2	1.1	4.1	a
	203.3	182.2	48.5	189.3	− 0.2	1.1	4.6	b
PdTi	169.8	150.3	44.7	156.8	− 0.2	1.1	4.6	a
	168.6	150.4	45.9	156.5	− 0.3	1.2	5.0	b
CuY	115.0	47.6	35.8	70.1	0.3	0.3	1.1	a
	114.3	47.1	36.7	69.5	0.3	0.3	1.1	b
	116.4	47.4	34.5	70.4	0.3	0.3	1.0	c[14]
	116.0	47.7	31.9	70.5	0.3	0.3	0.9	d[14]
AgY	98.1	53.3	35.5	68.2	0.1	0.5	1.6	a
	96.1	51.9	35.7	66.6	0.1	0.5	1.6	b
	105.3	50.3	37.2	68.6	0.2	0.4	1.4	c[14]
	102.4	54.5	32.6	70.5	0.2	0.4	1.4	d[14]

[a]This study (PAW, GGA-PW91).
[b]This study (PAW, GGA-PBE).
[c]Reported calculated results.
[d]Reported experimental results.

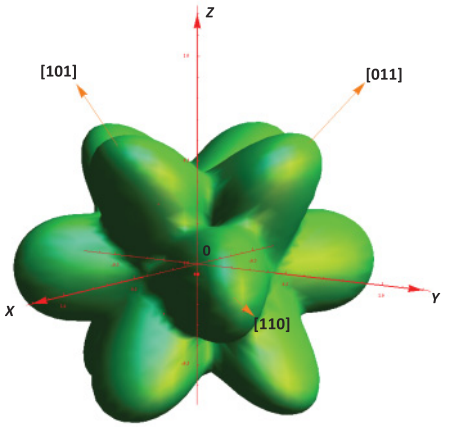

FIG. 2. (Color online) The variations in maximized PRs as a function of stretching directions as an isosurface for CuZr alloy. Each point on the surface represents the maximum value of the PRs for stretching the body along the n direction (i.e, α,β in a spherical coordinate system) passing through this point. The distance of the point from the origin is equal to the magnitude of the PRs.

get an extreme value of PRs with a certain proper u for a given stretch direction (α, β). Figure 2 shows an isosurface of the variation in maximized PRs as a function of α and β for CuZr. Each point on the surface represents the maximum value of the PR for stretching the body along the n direction (α, β in spherical coordinate system) passing through that point. The distance of the point from the origin is equal to the magnitude of this maximized PR. It is obvious that the maximum PR appears in ⟨110⟩ stretch directions, which is in accordance with others reports.[3,4] Thus, we can use simpler expressions derived by Baughman *et al*. to calculate the extreme PRs of the B2 intermetallics in terms of the elastic constants. They are given as follows:[4]

$$\begin{aligned} v_{\max} &= v([110],[001]) \\ &= \frac{4C_{12}C_{44}}{2C_{11}C_{44}+(C_{11}-C_{12})(C_{11}+2C_{12})}, \end{aligned} \tag{6}$$

$$\begin{aligned} v_{\min} &= v([110],[1\bar{1}0]) \\ &= -\frac{2C_{11}C_{44}-(C_{11}-C_{12})(C_{11}+2C_{12})}{2C_{11}C_{44}+(C_{11}-C_{12})(C_{11}+2C_{12})}. \end{aligned} \tag{7}$$

Equations (6) and (7) can measure the maximum and minimum PRs along the lateral directions when a [110] stretch is applied, respectively. Namely, if a stretch is applied along the face diagonal of the cubic cell, a maximum (compressive) and a minimum (either compressive or extensive) lateral strain will be detected along a perpendicular cube axis, and a perpendicular face-diagonal direction, respectively.

Table I and Table S list the extreme PRs for 142 B2 intermetallics obtained using Eqs. (6) and (7) with the calculated elastic moduli. The results show that more than 70% of the B2 intermetallics have negative PRs, suggesting that auxetic behavior is a common feature in B2 intermetallic compounds. Of the intermetallics listed in Table I, AuCd has the largest value of extreme PRs ($v_{\min} = -0.908$, $v_{\max} = 1.882$, GGA-PW91), while auxetic behavior does not occur in AlZr, CuY, and AgY.

C. Relationship between elastic anisotropy and extreme Poisson's ratios in B2 intermetallics

Generally, another index, A, is introduced to characterize the anisotropic elastic response in cubic crystals. It is given by the variation between C_{44} and $C' = C_{11} - C_{12}$ through the anisotropy ratio

$$A = \frac{2C_{44}}{C_{11}-C_{12}}. \tag{8}$$

The larger the value of A is, the more anisotropic the elastic response of the material is. When A reaches a minimum value of 1, then it is defined to indicate elastic isotropy. Walton's recent analysis[3] shows that a correlation exists between the value of the elastic anisotropy index and the magnitudes of maximum and minimum PRs in different solid materials. This correlation is independent of crystal symmetry and chemical nature of the materials. Moreover, negative Poisson's ratios occur in cubic materials in some combination of crystal load direction when $A > 3$ (Ref. 66) or 4.[3]

To test the validity of the elastic anisotropy index in B2 intermetallic compounds, we plotted the calculated maximum and minimum Poisson's ratios of 142 B2 intermetallic compounds against A in Fig. 3. Inspection of the figure reveals that a strong correlation exists between the extreme PRs and A. The extreme PRs all lie along two curves, which are approximately symmetrical with a single point of intersection at $A = 1.008$ (GGA-PW91), i.e., $v_{\max} = 0.329$ and $v_{\min} = 0.324$ for NiSc. Thus, we can make use of A as an auxetic index of B2 crystal structure.

According to our calculated data (see Table I and Table S), negative PRs can happen when A is larger than about 2.5. As expected, owing to the large fraction of the B2 intermetallics displaying auxetic behavior in comparison with other cubic materials, the required anisotropy ratio of about 2.5 is a smaller anisotropy than that seen in other auxetic cubic materials 3.[66] Of the intermetallic compounds investigated in this study, AuCd is the most anisotropic ($A = 45.17$, GGA-PW91),

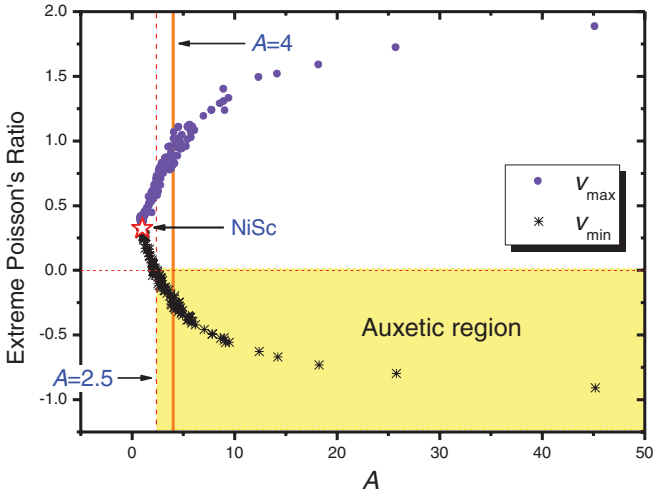

FIG. 3. (Color online) Plots of maximum and minimum Poisson's ratio against elastic anisotropy A for 144 B2 intermetallic compounds. The solid and dashed lines show $A = 4$ and 2.5, respectively.

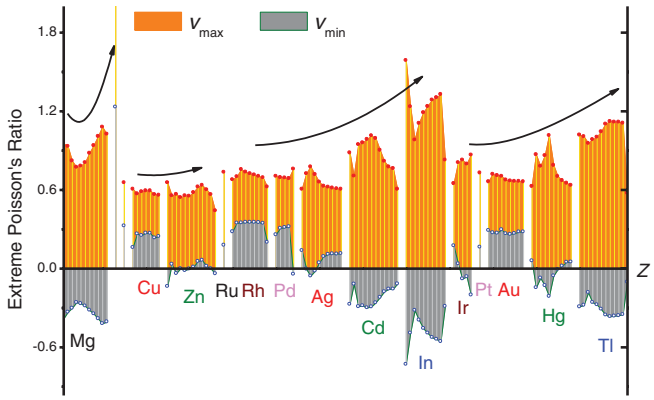

FIG. 4. (Color online) Relation of extreme Poisson's ratio to the periodic system of M (transition or main-group metal) elements for B2 RM intermetallics. The bars are grouped in blocks corresponding to a fixed M element, with the M elements labeled at the bottom of the figure with different colors. Within each M-element block, the bars are ordered by increasing atomic number of the R element (from Sc, Y, La, to Yb).

followed by AgCd alloy ($A = 25.77$, GGA-PW91), suggesting that they are intrinsically auxetic.

In an effort to extract more information about the auxetic nature of the B2 intermetallics, the extreme PRs of the RM B2 intermetallics were plotted as a function of atomic number of M (transition or main-group metal) elements, Z in Fig. 4. Each bar shows extreme PRs of a specific RM intermetallic. The bars are grouped in blocks corresponding to a fixed M element, with the M elements labeled at the bottom of the figure. Within each M-element block. the bars are ordered by increasing atomic number of the R element (from Sc, Y, La, to Yb). Obviously, the periodicity in the extreme PRs of the RM intermetallics in Fig. 4 is somewhat similar to that of the M-element electronic structure of atoms. As might be expected, in each period of the Periodic Table, maximum (minimum) Poisson's ratio tends to rise (fall) with increasing atomic number Z as electron shells and subshells gradually become filled in successive atoms, e.g, in RM alloys with M in the fifth period (M varying from Ru to In) of the Periodic Table, the average minimum (maximum) PRs of RRu and RRh is about 0.3 (0.65), while the average of maximum PRs for RIn increases (decreases) to about 1.2 (-0.58). Nonetheless, the relationship between extreme PRs and atomic number of R (rare-earth) elements is complex as a result of their configuration of $4f$ electron, as indicated by the different shapes for bars in Fig. 4. Regardless of the complexity of PRs in the B2 intermetallics with different R elements, the magnitudes of extreme PRs for RM intermetallics with different M elements in the same column of the Periodic Table are basically equal, and even the corresponding shapes of extreme PRs pillars display a similar feature, e.g., among the group 13 in Periodic Table, the maximum Poisson's ratio pillar for RIn and for RTl exhibit apparently the same profile, which tends to decrease first and then increase with an increase of rare-earth atomic number (from Sc, Y, La, to Yb). In Fig. 4, we can see that the B2 intermetallics consisting of groups 2, 12-13 metal elements and rare-earth elements can be auxetic. For instance, the B2 intermetallics containing Mg, In, and Tl in groups 2 and 13 have large absolute value of negative PRs with high anisotropy ratio ($A > 4$), which implies that they are auxetic.

D. Charge density topology and geometry and its relationship with extreme Poisson's ratios in B2 intermetallics

At this point, we turn our attention to the electronic origins of the extreme PRs, which can be described within the framework of QTAIM. QTAIM posits that solid-state structure, and hence properties, can be described in terms of the topology and geometry of the electron charge density, $\rho(\vec{r})$.[23,25,33,34] The theory capitalizes on the fact that $\rho(\vec{r})$ is a three-dimensional scalar field possessing a topology that is partially characterized by its rank-3 critical points (CPs). These are the points at which the field variable achieves extreme values in all three principal directions, i.e., the gradient of $\rho(\vec{r})$ vanishes. There are four kinds of rank-3 CP in a three-dimensional space: a local minimum, a local maximum, and two kinds of saddle points. These CPs are often denoted by an index that is the number of positive curvatures minus the number of negative curvatures. For example, a minimum CP has positive curvature in three orthogonal directions; therefore, it is a $(3, +3)$ CP. The first number is simply the number of dimensions of the space and the second is the net number of positive curvatures. A maximum is denoted by $(3, -3)$ because all three curvatures are negative. A saddle point with two of the three curvatures negative is denoted $(3, -1)$, while the other saddle point is a $(3, +1)$ CP.

Elements of solid-state structure and bonding correlate with the topological features of $\rho(\vec{r})$. In particular, a bond path is the ridge of maximum charge density connecting two nuclei. Its existence is guaranteed by the presence of a $(3, -1)$ CP, or bond CP, between two nuclei. Similarly, a $(3, +1)$ CP, or ring CP, is topologically required at the center of ring structures. Cage structures must enclose a single $(3, +3)$ CP, hence, these CPs are called a cage CP. The locations of the atomic nuclei always coincide with a maximum, a $(3, -3)$, or nuclear CP.

When we locate the CPs of $\rho(\vec{r})$ in the RM B2 intermetallics, we find that the only maxima are the atoms sitting at the vertices and the center of the unit cell, as shown for ScZn in Fig. 5. In this figure, the Zn atom is colored black and the Sc atoms are colored gray. These atoms are linked by nearest-neighbor Sc-Zn bond paths, shown as gray cylinders. The white circles in the figure represent cage points. These CPs can be seen to lie along the line connecting second-neighbor Zn atoms. When the material is deformed, charge will move between the Sc-Zn bonds and cages. It is the nature of this charge redistribution that mediates the maximum Poisson's ratios for a given material.

We have found that when a stretch applied in the $\langle 110 \rangle$ direction charge moves from the nearest-neighbor bond points into the surrounding cages as shown in Fig. 6. In this figure, the unfilled arrows represent the applied strain and the gray arrows represent the charge flow from the bond points to the cage point. This charge redistribution induces strains in the material. To understand the role of the charge redistribution on these strains, we can visualize the charge buildup in the cages and the depletion from the bonds as separate events, each of which accounts for a maximal strain in a different direction.

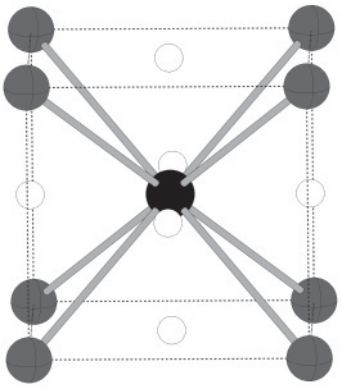

FIG. 5. The topology of ScZn. The Zn atom is shaded black, the Sc gray, and the cage points are shown with white circles. The gray cylinders represent the Sc-Zn bond paths, while the dashed lines show the edge of the unit cell.

First, we can consider the cage CPs. As the charge density in the cage point increases, we find that the distance between the second-neighbor atoms separated by the cage point decreases; these are the black atoms in Fig. 6. This observation is easily rationalized using the electrostatic theorem. At equilibrium, the repulsion of the second-neighbor atoms is exactly canceled by their attraction for the intervening density, i.e., that at the cage CP. As this density increases, so too does the attraction of the second-neighbor atoms to that density, resulting in a decrease in internuclear separation. This process gives rise to a positive $\upsilon_{\max}$ in the $\langle 001 \rangle$ direction. The magnitude of $\upsilon_{\max}$ will depend on the amount of charge redistribution. Materials that transfer a large amount of charge into the cage point will show a large $\upsilon_{\max}$, while those that do not will have a small $\upsilon_{\max}$.

In the second case, we must consider the effect of depleting electron density at the first-neighbor bond points. When the density between first-neighbor atoms is reduced, so too is the screening of their nuclear charges, which will tend to push first-neighbor atoms apart. This process leads to a small $\upsilon_{\min}$

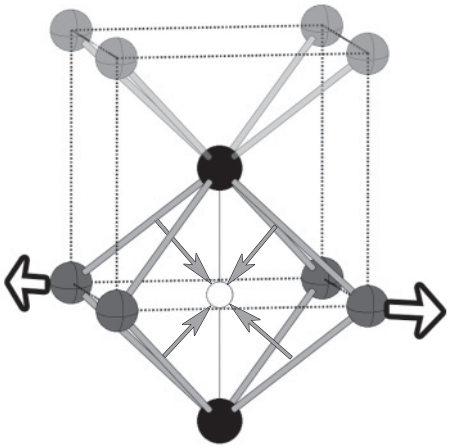

FIG. 6. The movement of charge from the bond points to the cage point in response to a strain applied in the $\langle 110 \rangle$ direction is shown by the gray arrows. The unfilled arrows represent the applied strain.

in the $\langle 1\bar{1}0 \rangle$ direction. If a sufficiently large amount of charge is removed from the bond points, $\upsilon_{\min}$ will become negative.

An interesting consequence of this picture is that it suggests there is a symmetry between $\upsilon_{\min}$ and $\upsilon_{\max}$ because both are due to the amount of charge that flows from the first-neighbor bond points to the cage points. Systems that redistribute a large amount of charge will have a large $\upsilon_{\max}$ and a negative $\upsilon_{\min}$. Systems that do not transfer charge easily between the bond and cage points will have a smaller $\upsilon_{\max}$ and a positive $\upsilon_{\min}$. This symmetry is, in fact, seen in Figs. 3 and 4.

The magnitude of the charge flow can be estimated using the directionality of the bond points, allowing the extreme Poisson's ratios to be predicted. Directionality has been quantified using the quadratic surface constructed from the Hessian of the charge density at the bond points.[23,33,34] This surface is the elliptic cone that surrounds the bond CP. Its extreme angles with respect to the plane normal to its axis are given by

$$\tan\theta = \rho_0 \sqrt{\frac{\rho_{\perp\perp}}{\rho_{\parallel\parallel}}}, \tag{9}$$

$$\tan\phi = \rho_0 \sqrt{\frac{\rho_{\perp'\perp'}}{\rho_{\parallel\parallel}}}, \tag{10}$$

where ρ_0 is charge density at the bond CP, $\rho_{\perp\perp}$ and $\rho_{\perp'\perp'}$ are the principal curvatures at the bond point in the directions perpendicular to the bond path, and $\rho_{\parallel\parallel}$ is the curvature along the bond path. In the B2 structure, the two perpendicular curvatures are degenerate, allowing directionality to be defined solely in terms of $\tan\theta$.

This definition of directionality is an approximate measure of the "distance" to bond breaking, i.e., the vanishing of the elliptic cone around the bond point, which will occur when the principal curvatures perpendicular to the bond path vanish. By definition, bond CPs with a small value of $\tan\theta$ are closer to a topological instability than systems with a large value of directionality, and the closer a bond CP is to a topological instability, the larger the magnitude of the charge flow from that bond CP for a given perturbation.[33,67,68] Thus, we expect that materials with directional bonds will have positive Poisson's ratios, while those with low values of directionality will have a negative Poisson's ratio in the $\langle 1\bar{1}0 \rangle$ direction.

To test this assertion, we plotted θ against $\upsilon_{\min}$ for the *RM* intermetallics investigated in this study (see Fig. 7). In this figure, crosses (circles) represent materials with a negative (positive) $\upsilon_{\min}$ and a vertical dashed line indicates where $\upsilon_{\min}$ vanishes. Inspection of the figure reveals that, as expected, $\upsilon_{\min}$ increases with directionality, i.e., materials with directional bonds have positive Poisson's ratios, while those with nondirectional bonds have a negative Poisson's ratio in the $\langle 1\bar{1}0 \rangle$ direction.

By viewing the extreme Poisson's ratios as arising from bond directionality, we can can begin to consider what types of orbitals give rise to auxetic behavior, an understanding of which would aid our ability to design new materials. The directionality of a compound's bond paths is determined by the type of filled orbitals that participate in bond formation. Only those orbitals that can increase density along the bond path will increase directionality. In the O_h point group, these would be the *d* orbitals transforming as T_{2g}, along with the

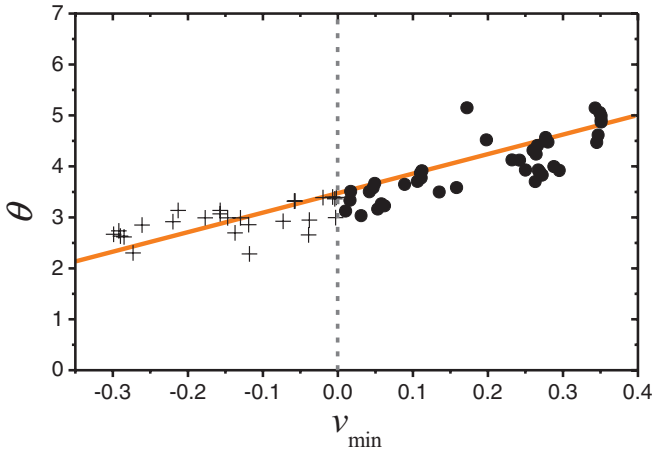

FIG. 7. (Color online) Plot of θ against υ_{min} for the RMs investigated in this study. Crosses (circles) indicate compounds with a negative (positive) υ_{min}. A vertical dashed line is used to show where υ_{min} is zero. The solid straight line serves as a guide for the eye.

p and f orbitals transforming as T_{1u}, at the band Γ point. All other orbitals will serve to decrease the directionality. This picture explains why pure bcc metals that bond using primarily s density (e.g., Li, Na, K, Rb) are auxetic.[56] It also predicts that the RMg intermetallics studied here should have a negative υ_{min}, a fact that is easily verified by examining Fig. 4. If, however, we consider Rh, which has partially filled d orbitals, we find that the RRhs have positive Poisson's ratios (Fig. 4). This approach provides a new means of understanding the electronic origins of auxetic behavior in B2 intermetallics and may provide insight to aid in the design of such materials.

IV. CONCLUSIONS

In summary, we have systematically investigated the elastic properties of a series of B2 intermetallic compounds using first-principles calculations, and have derived the extreme Poisson's ratios of 142 B2 intermetallics, including 14 non-rare-earth- and 128 rare-earth-metal B2 intermetallics. We used these data to predict that 70% of the B2 alloys presented here are auxetic, and more than one third of them have strong auxetic behavior. We also found that the extreme Poisson's ratios (both positive and negative) are strongly correlated with elastic anisotropy. Finally, we analyzed the electron charge density of these intermetallics and found that materials whose bonding has a strong angular dependence are not auxetic, whereas materials whose bonds lack an angular dependence are auxetic.

ACKNOWLEDGMENT

This work was supported by the Natural Science Foundation of Hunan Province for Innovation Group (Grant No. 09JJ7004), the Key Special Program for Science and Technology of Hunan Province (Grant No. 2009FJ1002), the Natural Science Foundation of China (Grants No. 10872177 and No. 10972190), and the US Army Research Office under 421-20-18.

*trjones@mines.edu
†zhouyc@xtu.edu.cn

[1] K. Evans and A. Alderson, Adv. Mater. **12**, 617 (2000).
[2] W. Yang, Z. M. Li, W. Shi, B. H. Xie, and M. B. Yang, J. Mater. Sci. **39**, 3269 (2004).
[3] Z. A. D. Lethbridge, R. I. Walton, A. S. H. Marmier, C. W. Smith, and K. E. Evans, Acta Mater. **58**, 6444 (2010).
[4] R. H. Baughman, J. M. Shacklette, A. A. Zakhidov, and S. Stafstrom, Nature (London) **392**, 362 (1998).
[5] L. Rothenburg, A. A. Berlin, and R. J. Bathurst, Nature (London) **354**, 470 (1991).
[6] N. Gaspar, X. J. Ren, C. W. Smith, J. N. Grima, and K. E. Evans, Acta Mater. **53**, 2439 (2005).
[7] Y. N. Zhang, R. Q. Wu, H. M. Schurter, and A. B. Flatau, J. Appl. Phys. **108**, 023513 (2010).
[8] R. H. Baughman, S. O. Dantas, S. Stafstrom, A. A. Zakhidov, T. B. Mitchell, and D. H. E. Dubin, Science **288**, 2018 (2000).
[9] X. Huang, G. J. Ackland, and K. M. Rabe, Nat. Mater. **2**, 307 (2003).
[10] G. H. Cao, A. T. Becker, D. Wu, L. S. Chumbley, T. A. Lograsso, A. M. Russell, and K. A. Gschneidner Jr., Acta Mater. **58**, 4298 (2010).
[11] Q. Chen and S. B. Biner, Acta Mater. **53**, 3215 (2005).
[12] J. R. Morris, Y. Ye, Y. B. Lee, B. N. Harmon, K. A. Gschneidner Jr., and A. M. Russell, Acta Mater. **52**, 4849 (2004).
[13] R. P. Mulay, J. A. Wollmershauser, M. A. Heisel, H. Bei, A. M. Russell, and S. R. Agnew, Acta Mater. **58**, 2788 (2010).
[14] K. A. Gschneidner Jr., A. Russell, A. Pecharsky, J. Morris, Z. Zhang, T. Lograsso, D. Hsu, C. Chester Lo, Y. Ye, A. Slager *et al.*, Nat. Mater. **2**, 587 (2003).
[15] N. Hatcher, O. Y. Kontsevoi, and A. J. Freeman, Phys. Rev. B **80**, 144203 (2009).
[16] M. F. X. Wagner and W. Windl, Acta Mater. **56**, 6232 (2008).
[17] Y. Wu, Y. Xiao, G. Chen, C. T. Liu, and Z. Lu, Adv. Mater. **22**, 2770 (2010).
[18] S. Pauly, S. Gorantla, G. Wang, U. Kuhn, and J. Eckert, Nat. Mater. **9**, 473 (2010).
[19] D. C. Hofmann, Science **329**, 1294 (2010).
[20] K. A. Gschneidner Jr., M. Ji, C. Z. Wang, K. M. Ho, A. M. Russell, Y. Mudryk, A. T. Becker, and J. L. Larson, Acta Mater. **57**, 5876 (2009).
[21] M. E. Eberhart, Acta Mater. **44**, 2495 (1996).
[22] T. E. Jones, M. E. Eberhart, D. P. Clougherty, and C. W. Woodward, Phys. Rev. Lett. **10**, 085505 (2008).
[23] N. Kioussis, M. Herbranson, E. Collins, and M. E. Eberhart, Phys. Rev. Lett. **88**, 125501 (2002).
[24] M. Eberhart, Phys. Rev. Lett. **8720**, 205503 (2001).
[25] T. E. Jones, M. E. Eberhart, and D. P. Clougherty, Phys. Rev. Lett. **105**, 265702 (2010).
[26] P. Hohenberg and W. Kohn, Phys. Rev. B **136**, 864 (1964).
[27] P. N. H. Nakashima, A. E. Smith, J. Etheridge, and B. C. Muddle, Science **331**, 1583 (2011).

[28]R. F. W. Bader, *Atoms in Molecules. A Quantum Theory* (Clarendon, Oxford, 1990).
[29]R. Bader, Rep. Prog. Phys. **44**, 52 (1981).
[30]T. E. Jones and M. E. Eberhart, Int. J. Quantum Electron. **110**, 1500 (2010).
[31]T. E. Jones and M. E. Eberhart, J. Chem. Phys. **130**, 204108 (2009).
[32]T. E. Jones, M. E. Eberhart, S. Imlay, and C. Mackey, J. Phys. Chem. A **115**, 12582 (2011).
[33]M. E. Eberhart and A. F. Giamei, Mater. Sci. Eng., A **248**, 287 (1998).
[34]T. E. Jones, M. E. Eberhart, and D. P. Clougherty, Phys. Rev. Lett. **100**, 017208 (2008).
[35]M. E. Eberhart, D. P. Clougherty, and J. M. MacLaren, Philos. Mag. B **68**, 455 (1993).
[36]G. Kresse and J. Furthmuller, Phys. Rev. B **54**, 11169 (1996).
[37]W. Kohn and L. J. Sham, Phys. Rev. A **140**, 1133 (1965).
[38]G. Kresse and D. Joubert, Phys. Rev. B **59**, 1758 (1999).
[39]H. Zhang, S. Shang, J. E. Saal, A. Saengdeejing, Y. Wang, L. Q. Chen, and Z. K. Liu, Intermetallics **17**, 878 (2009).
[40]M. C. Gao, A. D. Rollett, and M. Widom, Phys. Rev. B **75**, 174120 (2007).
[41]G. Kresse and J. Furthmuller, Comput. Mater. Sci. **6**, 15 (1996).
[42]J. P. Perdew and Y. Wang, Phys. Rev. B **45**, 13244 (1992).
[43]J. P. Perdew, K. Burke, and M. Ernzerhof, Phys. Rev. Lett. **77**, 3865 (1996).
[44]M. C. Gao, A. D. Rollett, and M. Widom, CALPHAD **30**, 341 (2006).
[45]H. J. Monkhorst and J. D. Pack, Phys. Rev. B **13**, 5188 (1976).
[46]M. Mattesini, R. Ahuja, and B. Johansson, Phys. Rev. B **68**, 184108 (2003).
[47]S. Q. Wang and H. Q. Ye, J. Phys.: Condens. Matter **15**, 5307 (2003).
[48]TECPLOT, http://www.tecplot.com/.
[49]G. Ghosh, Acta Mater. **55**, 3347 (2007).
[50]G. Ghosh, S. Delsante, G. Borzone, M. Asta, and R. Ferro, Acta Mater. **54**, 4977 (2006).
[51]G. Bihlmayer, R. Eibler, and A. Neckel, Phys. Rev. B **50**, 13113 (1994).
[52]G. Ghosh and M. Asta, Acta Mater. **53**, 3225 (2005).
[53]O. Mercier, K. N. Melton, G. Gremaud, and J. Hagi, J. Appl. Phys. **51**, 1833 (1980).
[54]P. Young and A. Bienenstock, J. Appl. Phys. **42**, 3008 (1971).
[55]G. M. Mcmanus, Phys. Rev. **129**, 2004 (1963).
[56]R. Goldstein, V. Gorodtsov, and D. Lisovenko, Mech. Solids **45**, 529 (2010).
[57]J. R. J. Schiltz, T. S. Prevender, and J. F. Smith, J. Appl. Phys. **42**, 4680 (1971).
[58]See Supplemental Material at http://link.aps.org/supplemental/10.1103/PhysRevB.85.134108 for a table of the calculated elastic constants of the 128 B2 *RM* intermetallics.
[59]G. L. Zhao and B. N. Harmon, Phys. Rev. B **48**, 2031 (1993).
[60]T. Makita, A. Nagasawa, Y. Morii, N. Minakawa, and H. Ohno, Phys. B (Amsterdam) **213-214**, 430 (1995).
[61]T. Ohba, Phase Transitions **69**, 289 (1999).
[62]X. Huang, K. M. Rabe, and G. J. Ackland, Phys. Rev. B **67**, 024101 (2003).
[63]O. Gülseren and R. E. Cohen, Phys. Rev. B **65**, 064103 (2002).
[64]Y. Wang, J. Wang, H. Zhang, V. Manga, S. Shang, L. Q. Chen, and Z. Liu, J. Phys.: Condens. Matter **2**, 225404 (2010).
[65]J. P. Perdew, J. A. Chevary, S. H. Vosco, K. A. Jackson, M. R. Pederson, D. J. Singh, and C. Fiolhais, Phys. Rev. B **46**, 6671 (1992).
[66]T. Paszkiewicz and S. Wolski, Phys. Status Solidi B **244**, 966 (2007).
[67]P. Ayers and S. Jenkins, J. Chem. Phys. **130**, 154104 (2009).
[68]A. Guevara-García, E. Echegaray, A. Toro-Labbe, S. Jenkins, S. Kirk, and P. W. Ayers, J. Chem. Phys. **134**, 234106 (2011).